

Gas-phase velocity estimation in practical sprays by Phase-Doppler technique

Erika Rácz^a, Milan Malý^b, Jan Jedelský^b, Viktor Józsa^{a,*}

^a Department of Energy Engineering, Faculty of Mechanical Engineering, Budapest University of Technology and Economics, Műegyetem rkp. 3., H-1111 Budapest, Hungary

^b Faculty of Mechanical Engineering, Brno University of Technology, Technická 2896/2, 616 69 Brno, Czech Republic

ARTICLE INFO

Keywords:

atomization
Phase Doppler
velocity
Stokes number
droplet
spray

ABSTRACT

Practical sprays are characterized by a two-way coupling between droplets and the surrounding gas. The effect of sprays on process performance is critical in numerous applications; hence, the gas-phase velocity is often estimated via two methods, using Phase Doppler measurement data. The first one is using a rule of thumb, i.e., estimating the gas-phase velocity by analyzing droplet sizes below a few micrometers. The second way of estimating the Stokes number, Stk , is using a threshold well below unity, such as 0.1. There are numerous definitions available in the literature for Stk , resulting in several magnitudes difference. These complex problems are resolved in this paper in the following way. A new definition for Stk is provided, which is sufficiently robust for, e.g., pressure and twin-fluid atomizers. According to the results, the $Stk < 0.1$ threshold means droplet sizes between 2 and 10 micrometers above 10 m/s gas-phase velocities. Filtering for too small droplets could lead to biased characteristics, especially in estimating the turbulent properties. Hence, the gas-phase velocity estimation is a function of the measurement setup and has a significant spatial dependence. The reader can find the software code online and the algorithm in Appendix A.

1. Introduction

The driving force of intense research in liquid fuels is the 100 EJ problem (Hannula and Reiner, 2019), which was the global energy used for transportation in 2014. Moreover, the electricity price will be significantly higher if combustion systems are omitted, even at zero allowed CO₂ emission (Sepulveda et al., 2018). Since transportation is tough to decarbonize (de Blas et al., 2020), renewable liquid fuels are desired to be used with our current injection systems and combustion chambers in the transitory decades to reduce our carbon footprint (Chiong et al., 2018). However, atomizing renewable liquid fuels is more complicated than conventional fuels (Broumand et al., 2020). Besides combustion, sprays are used in numerous industries, from cooling through agriculture to medicine (Nasr et al., 2002). Droplet formation in twin-fluid and pressure atomizers results from the intense momentum transfer between a liquid jet or film and the surrounding continuous phase, which is air in most practical cases. The surrounding gas interacts with the spray, and a two-way coupling is established, i.e., the velocity field of the air stream is affected by the spray and vice versa, especially if the flow is turbulent. Numerical simulation validation requires

measuring velocity field besides droplet size distribution at characteristic points (Berni et al., 2022), while the turbulent fluctuations can also be critical (Collin-Bastiani et al., 2021).

The phase Doppler technique is the most suitable experimental tool for acquiring the required information on sprays, which simultaneously measures the size and velocity of spherical droplets (Albrecht et al., 2003). Depending on the design and the local atomization conditions, a single droplet bears either higher or lower velocity than the surrounding air, which a particle with zero inertia would only follow. Such a particle does not exist; moreover, the lower detection limit of the Phase Doppler anemometer (PDA) system equals the wavelength of the used laser, usually 0.5–0.8 μm. The upper threshold must be determined to ensure practically unbiased one-way coupling between the continuous phase and the particles (Elghobashi, 1994). To end up with a statistically significant number of tiny droplets for various quantities of interest, it is desired to set the threshold of the low-pass size filter as high as possible. There is no general theory or a rule of thumb for what is sufficiently large; it ranges from thousands (Menon and Gurunadhan, 2022) to tens of thousands (Chong and Hochgreb, 2015) in research papers. However, based on preliminary tests, information theory might facilitate solving this problem (Panão, 2020). Evidently, the number of required droplets

* Corresponding author.

E-mail address: jozsa@energia.bme.hu (V. Józsa).

<https://doi.org/10.1016/j.ijmultiphaseflow.2022.104260>

Received 15 May 2022; Received in revised form 10 August 2022; Accepted 16 September 2022

Available online 17 September 2022

0301-9322/© 2022 The Author(s). Published by Elsevier Ltd. This is an open access article under the CC BY license (<http://creativecommons.org/licenses/by/4.0/>).

Nomenclature*Latin letters*

Notation	Description (Unit –if relevant)
AB	airblast atomizer
b	number of bins
d_h	hydraulic diameter of the nozzle (m)
D	droplet diameter (m)
EFF-OIG	effervescent atomizer, out-in-gas setup
EFF-OIL	effervescent atomizer, out-in-liquid setup
GLR	gas-to-liquid mass flow ratio (–)
l	characteristic length (m)
LHO	light heating oil
n	number of droplets
p	pressure (bar)
PS	pressure-swirl atomizer
RO	crude rapeseed oil
Stk	Stokes number (–)
T	temperature (°C)
v	velocity (m/s)
v'	fluctuating velocity component (m/s)

Subscripts

Notation	Description
0.01	at Stk = 0.01
0.1	at Stk = 0.1
1	at Stk = 1
crit	critical
D	droplet
f	flow
g	gas
l	liquid
mean	mean value
rel.std	relative standard deviation
std	standard deviation

Greek letters

Notation	Description (Unit – if relevant)
μ	dynamic viscosity (Pa·s)
ρ	density (kg/m ³)
τ	time (s)

depends on the information gathered from the data, i.e., more data is necessary for root mean square velocity calculation than for estimating the mean velocity due to the second power of the individual droplets.

Practical atomizers produce either a narrow or a wide size range, but it is against the laws of physics to have a spray with only small or large droplets besides the mid-size zone (Babinsky and Sojka, 2002). Therefore, as a rule of thumb, filtering the data to a certain droplet size might lead to too few droplets. Such values range from 0.9 μm (Xiao et al., 2014) for artificial particles to 5 μm (Ferrand et al., 2003; Wu et al., 2022) for droplets, but 10 μm (Kourmatzis et al., 2013) and even 30 μm (Pakhomov and Terekhov, 2020a) can be found in the literature. It is known that the Stokes number, Stk, should be well below unity for droplets to be good tracers, ranging from 0.05 (Kourmatzis et al., 2013) to 0.5 (Temme et al., 2014). However, the further problem is that there is no generally applicable definition beyond the particle-to-flow time scale, τ_D/τ_f (Lau and Nathan, 2016). The definition of the former is clear,

while that of the flow time scale varies. There is a definition for jet flows (Ferrand et al., 2003), while it cannot be used for, e.g., pressure-swirl atomizers. A simple approach is to use the particle size as a characteristic flow length scale, which inherently leads to enormous Stk values (Feng et al., 2019). This, however, does not ultimately mean that they poorly follow the bulk flow. Suppose the distance from the nozzle is considered as the characteristic length (Jedelsky and Jicha, 2014). In that case, Stk could be large in the vicinity of the nozzle, especially if a two-phase jet is discharged with no further atomization downstream. In contrast, Stk could be too small for large droplets far from the nozzle. The characteristic flow length scale is easy to determine numerically (Pakhomov and Terekhov, 2020b). However, high-fidelity numerical simulation of atomization at system scale is expensive, not to mention reactive flows. Moreover, the numerical data must be validated by experiments. An empirical estimation for the time scale can be derived from the turbulent kinetic energy and the dissipation rate (Sommerfeld and Kussin, 2003), needing Particle Image Velocimetry, PIV, measurements (Li et al., 2021; Xu and Chen, 2013). There is an example for using the cell size as a characteristic length (Gerbino et al., 2021); however, it makes Stk a mesh-dependent quantity.

The novelty of this paper is the revision of PDA data sets of several atomizers to determine the critical droplet size, D_{crit} , up to which the mean droplet velocity, v_{mean} , represents the gas-phase velocity, v_g . For this purpose, a new definition for Stk was introduced, which is directly applicable to all pressure and twin-fluid atomizers. To justify the proposed Stk threshold, v_{mean} and standard deviation of the droplet velocity, v_{std} , were analyzed. The final result is a simple and robust method that can be employed to determine D_{crit} for most practical atomizers to characterize the flow field and the interaction between the spray and the continuous medium. Besides smooth velocity profiles in the mainstream, peripheral regions are also evaluated, where the size and velocity distributions are less regular, and the determination of v_g is rather

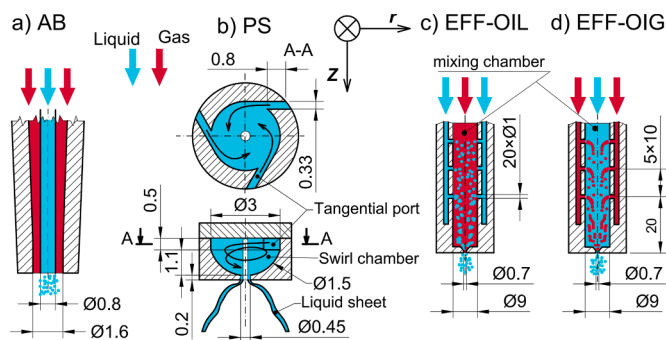


Fig. 1. The geometry of the previously investigated atomizers. a) airblast, b) pressure-swirl, effervescent with c) out-in-liquid, and d) out-in-gas configurations (Jedelsky et al., 2018; Urbán et al., 2019; Zaremba et al., 2018, 2017).

Table 1

The evaluated test conditions in the present paper.

Atomizer	Liquid(s)	GLR	p_g/p_l [bar]	T [°C]	r/z [mm]	d_h [mm]	sample size	Ref.
AB	diesel, LHO, RO, Water	0.78–2.36	0.3–2.4/0.01	25–100	0–14/20–60	0.4	40.000	(Urbán et al., 2019)
PS	Jet A-1	–	–/5–15	20	0–48/12.5–50	0.45	100.000	(Jedelsky et al., 2018)
EFF-OIL	LHO	0.025–0.1	0.7/0.7	23	0–20/5–80	0.7	30.000	(Zaremba et al., 2018)
EFF-OIG	LHO	0.025–0.2	0.35–2.8/0.35–2.8	23	0–21/100	0.7	20.000	(Zaremba et al., 2017)

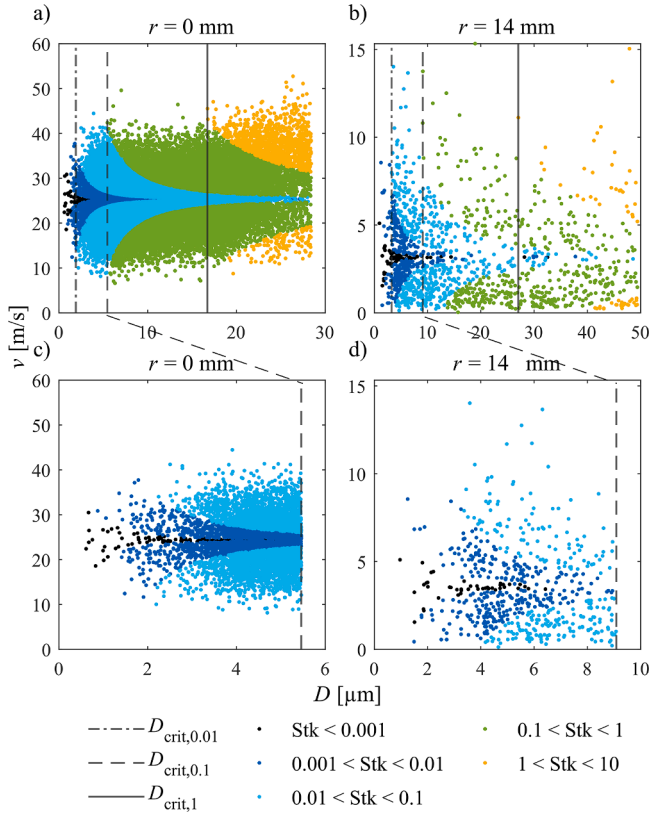


Fig. 2. Droplet size-velocity distribution for diesel, $p_g = 0.3$ bar, $T = 25$ °C, and $z = 60$ mm. a) $r = 0$ mm b) $r = 14$ mm, c) $r = 0$ mm filtered by $D_{crit,0.1}$ and d) $r = 14$ mm filtered by $D_{crit,0.1}$.

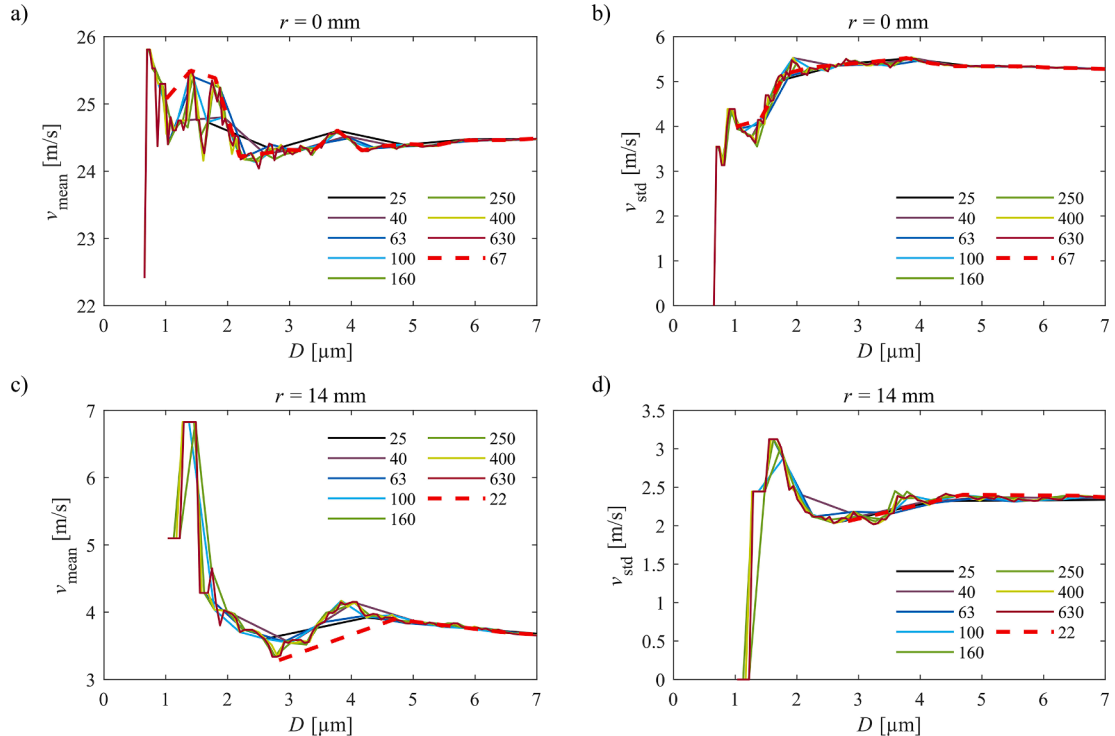


Fig. 3. v_{mean} and v_{std} of droplet classes up to an increasing droplet diameter with various droplet class numbers. Diesel fuel, $p_g = 0.3$ bar, $T = 25$ °C, and $z = 60$ mm. a) v_{mean} at $r = 0$ mm, b) v_{std} at $r = 0$ mm, c) v_{mean} at $r = 14$ mm, and d) v_{std} at $r = 14$ mm.

challenging. The Matlab software code for D_{crit} determination is available on the home page of our research group (Rácz and Józsa, 2022), and the algorithm can be found in Appendix A.

2. Materials and methods

This section is divided into two parts. Firstly, the evaluated atomizers are presented, which were investigated in earlier works. Their PDA measurement data are re-evaluated to test a proposed method for D_{crit} estimation. The selected conditions were highlighted, focusing on various spray regimes. The second subsection details data filtering and Stk estimation, emphasizing the comparison with alternative definitions available in the literature.

2.1. The evaluated atomizers

Figure 1 shows the geometry of all atomizers investigated in the preceding papers by the authors. The analyzed setup parameters and measurement locations are included in Table 1. The airblast atomizer, AB, is shown in Fig. 1a, which was used to establish the hypothesis on D_{crit} estimation. The first obvious choice for comparison was the pressure-swirl atomizer, PS, due to its popularity in practical applications, and its operation is notably different from AB. The last atomizer considered in this study is effervescent in two configurations. In the first case, the liquid was introduced from outside, called out-in-liquid, EFF-OIL. The second configuration is the reverse; the air is introduced to the chamber from outside, called out-in-gas, EFF-OIG.

The atomized liquids for the evaluated setups were: standard diesel fuel, EN590:2017, light heating oil, LHO, crude rapeseed oil, RO, distilled water, and commercial aviation kerosene, type Jet A-1. The spray quality of twin-fluid atomizers is primarily affected by the gas-to-liquid mass flow ratio, GLR . While this property was in the range of unity for AB, its value for EFF was a magnitude lower. This is the advantage of EFF atomizers over other twin-fluid atomizers, i.e., they consume a fraction of auxiliary gas needed for an acceptable spray quality. The

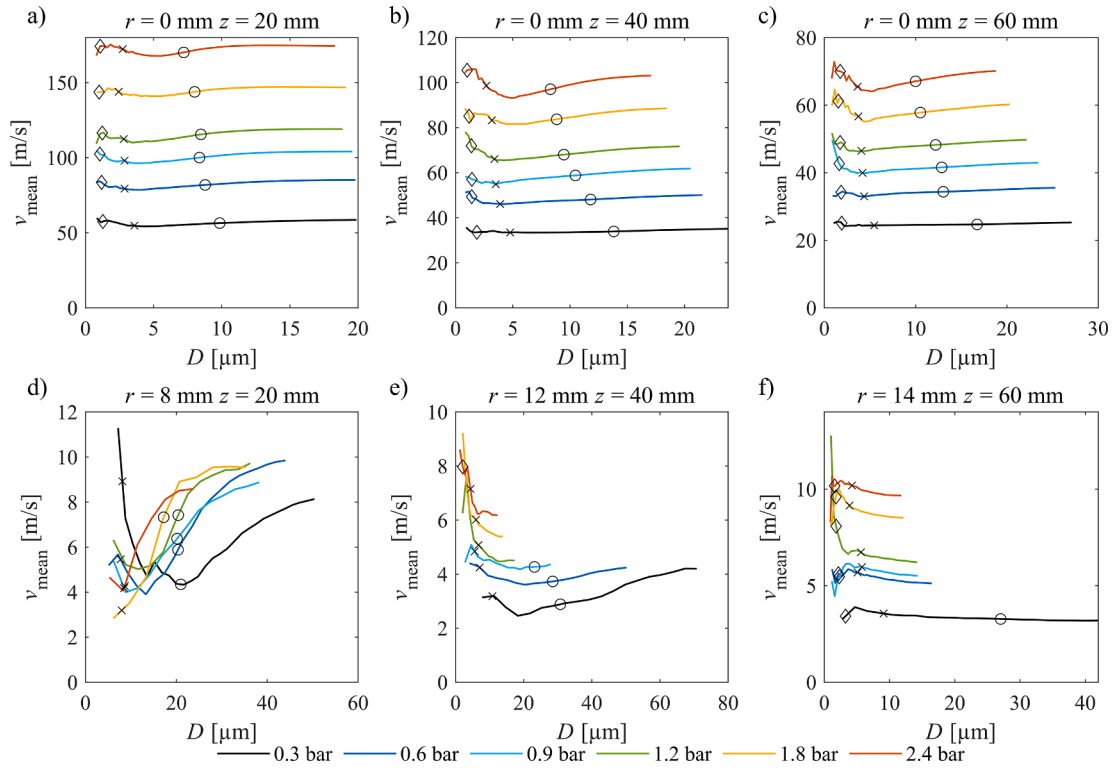


Fig. 4. v_{mean} of droplet classes up to an increasing diameter value at various p_g at $r = 0$ mm and a) $z = 20$ mm, b) $z = 40$ mm, and c) $z = 60$ mm. $r = 14$ mm and d) $z = 20$ mm, e) $z = 40$ mm, and f) $z = 60$ mm. Markers: $\diamond D_{\text{crit},0.01}$, $\times D_{\text{crit},0.1}$, and $\circ D_{\text{crit},1}$.

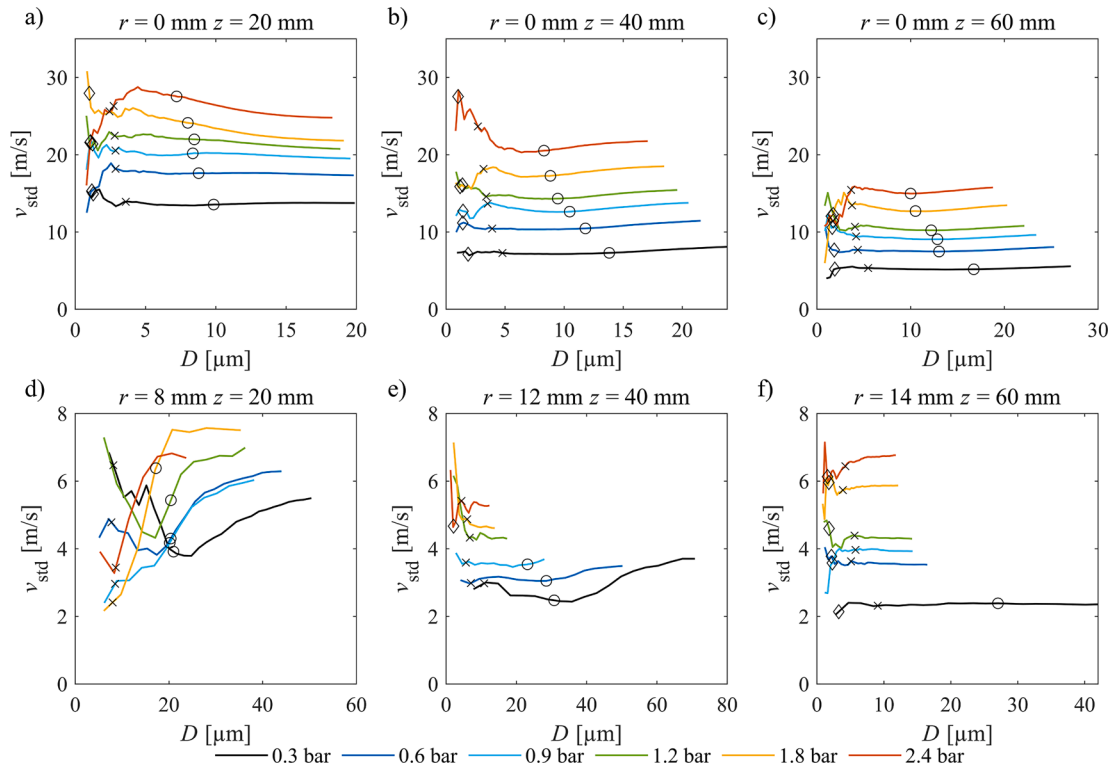


Fig. 5. v_{std} of droplet classes up to an increasing diameter value at various p_g at $r = 0$ mm and a) $z = 20$ mm, b) $z = 40$ mm, and c) $z = 60$ mm. $r = 14$ mm and d) $z = 20$ mm, e) $z = 40$ mm, and f) $z = 60$ mm. Markers: $\diamond D_{\text{crit},0.01}$, $\times D_{\text{crit},0.1}$, and $\circ D_{\text{crit},1}$.

gauge pressures of gas, p_g , and liquid, p_l are also indicated. The former parameter is irrelevant for PS. The liquid temperature, T , was only varied in the case of AB. The fifth column contains the radial, r , and the

axial coordinate, z , of the evaluated PDA data sets, measured from the nozzle tip. The hydraulic diameter, d_h , of the nozzles is also added, a key parameter for Stk estimation, detailed in [Subsection 2.2](#).

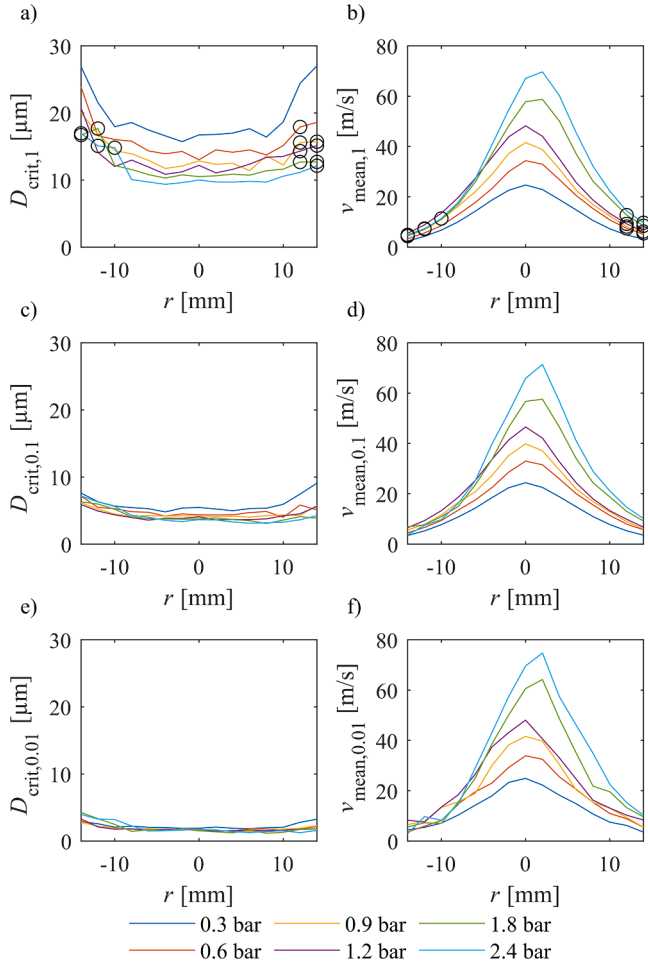


Fig. 6. The critical droplet size of a diesel spray along a diameter at $T = 25^\circ\text{C}$ and $z = 60\text{ mm}$, and v_{mean} with various D_{crit} values. \circ shows the largest droplet size, where $\text{Stk} = 1$ was not reached.

2.2. Data processing and Stokes number estimation

The PDA system was identical for all measurements, meaning a consistent database. Only the sensitivity was varied, depending on spray characteristics, to avoid saturation of the photomultiplier tube by large droplets and to detect the smallest ones. Since the wavelength of the used Ar-ion laser was 514.5 nm, all data below this size was removed since the processor only determines the size from this signal. The second velocity component was measured by a blue beam with a wavelength of 488 nm. Excessively large, unrepresentative droplets were filtered out by the *isoutlier* Matlab function (MathWorks, 2020) that uses the triple of the median absolute deviations. These two combined processes are called pre-filtering, which removed 10-20% of the data, depending on the conditions. This value is lower at the mainstream with more regular size distributions, while relatively more data was rejected on the periphery. The principal reason is the long tails of the distributions on the right side (Urbán et al., 2020a).

These atomizers produced a sufficiently large number of droplets to achieve a several kHz mean sampling frequency in the mainstream. The sample size must be sufficiently large to represent the relevant statistical properties of the variables. However, the temporal signal was still too noisy to identify the small passing vortices even after filtering. Therefore, the determined v_g is respective to the sample size, which is acceptable for continuously operating nozzles. The system was configured to record the data for either 15 s for AB or 60 s for the other atomizers. The required samples were acquired in the dense spray region

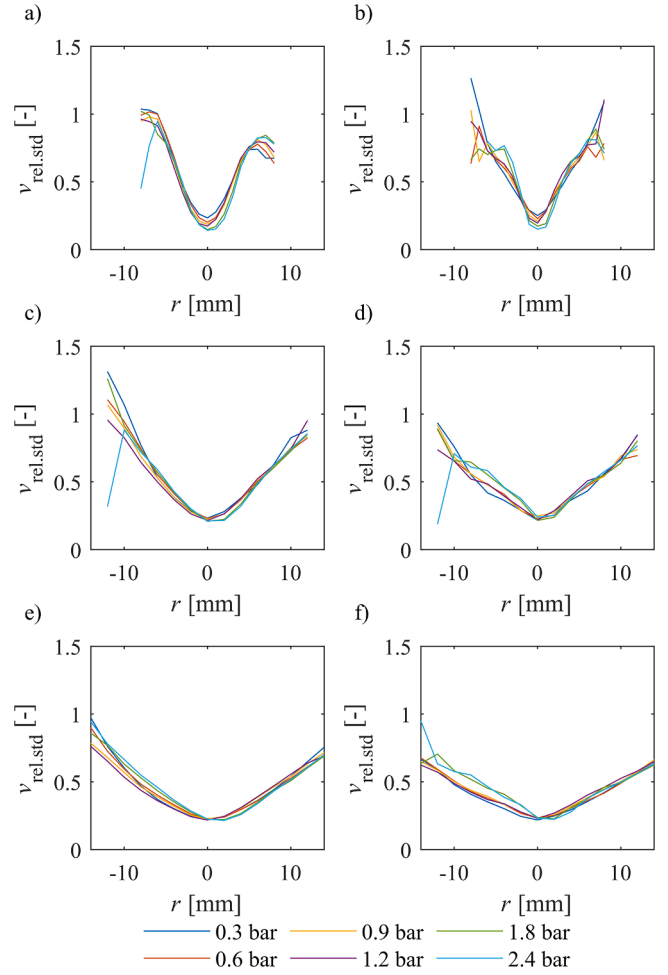


Fig. 7. $v_{\text{rel,std}}$ of a diesel spray along a diameter at $T = 25^\circ\text{C}$. a) unfiltered data at $z = 20\text{ mm}$, b) filtered data with $D_{\text{crit},0.1}$ at $z = 20\text{ mm}$, c) unfiltered data at $z = 40\text{ mm}$, d) filtered data with $D_{\text{crit},0.1}$ at $z = 40\text{ mm}$, e) unfiltered data at $z = 60\text{ mm}$, f) filtered with $D_{\text{crit},0.1}$ data at $z = 60\text{ mm}$.

within a few seconds. The peripheral regions usually contain a low number of droplets; hence, the temporal constraints ended the measurements here.

D_{crit} was determined based on the Stk . The best threshold was reached at $\text{Stk} = 0.1$, noted further as $D_{\text{crit},0.1}$, which choice will be justified in Subsection 3.1. Stk was calculated as:

$$\text{Stk} = \frac{|v_g - v_D| \cdot \rho_l \cdot D^2}{18 \cdot \mu_g \cdot l}, \quad (1)$$

where v_g is to be determined; consequently, an iteration loop was required, using v_{mean} as the starting value. v_D is the absolute droplet velocity calculated from the two velocity components. Hence, $|v_g - v_D|$ is the relative velocity between the actual droplet and the gas phase. ρ_l is the liquid density, D is the droplet diameter, and μ_g is the dynamic viscosity of the gas phase. l is the characteristic length which is the most controversial parameter in Eq. (1), emphasized in the third paragraph of the Introduction.

Many papers use a geometric size independent of the atomizer geometry as l , implying different results for various setups. Moreover, if the spray is discharging into the open atmosphere, e.g., in the case of spray gates, the flow is not bounded. The choice of the droplet size could be problematic since the velocity of a droplet will not be relaxed over the length of the droplet diameter. Since the flow field will be measured, only numerical simulations can estimate l with high accuracy; however, the results need to be validated, which leads back to measurements. To

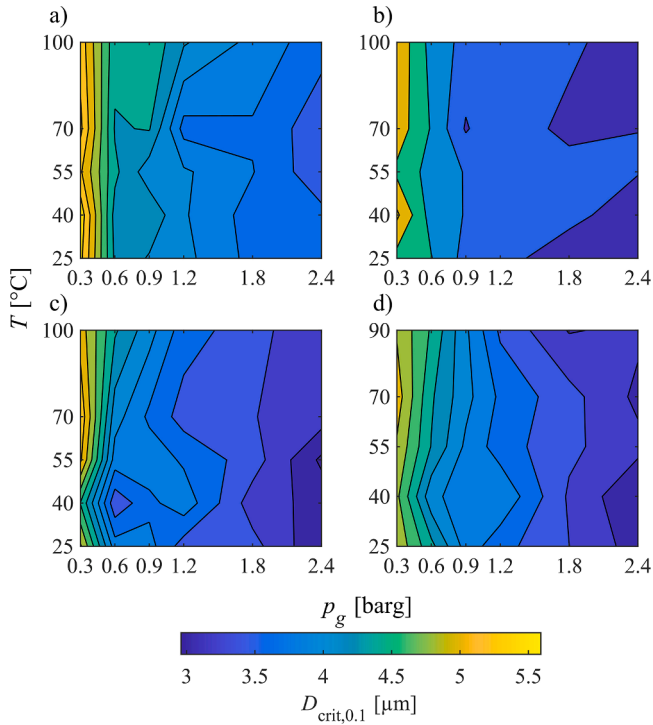


Fig. 8. Effect of liquid temperature and p_g on $D_{crit,0.1}$ at $r = 0$ mm and $z = 60$ mm for a) diesel fuel, b) LHO, c) RO, and d) water.

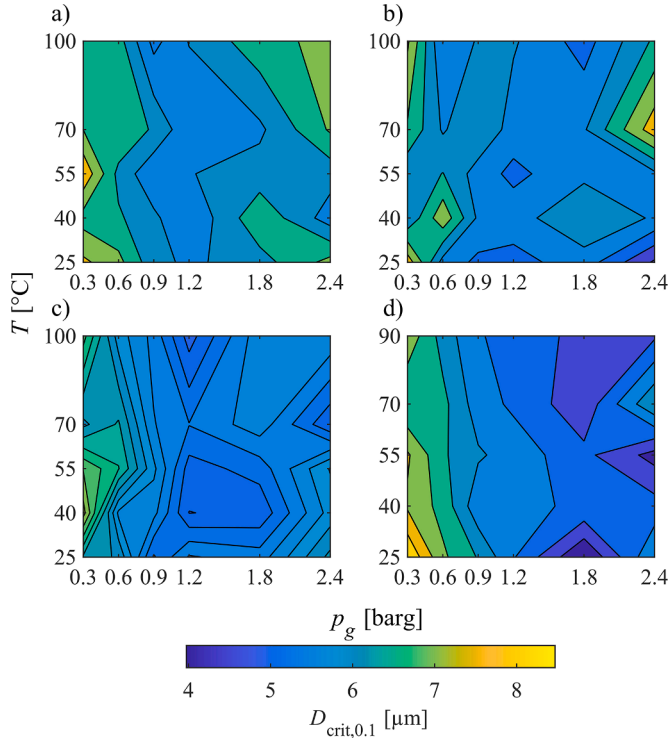


Fig. 9. Effect of liquid temperature and p_g on $D_{crit,0.1}$ at $r = 14$ mm and $z = 60$ mm for a) diesel fuel, b) LHO, c) RO, and d) water.

break this circle, estimation of l was approached from free jet theory since AB and PS atomizers generate the droplets via velocity difference, i.e., $|v_g - v_D|$, between the gaseous and the liquid media by injecting one, as a high-velocity jet, into the other. This step is essential since if the definition of l is confined to the gaseous phase, Eq. (1) cannot be used

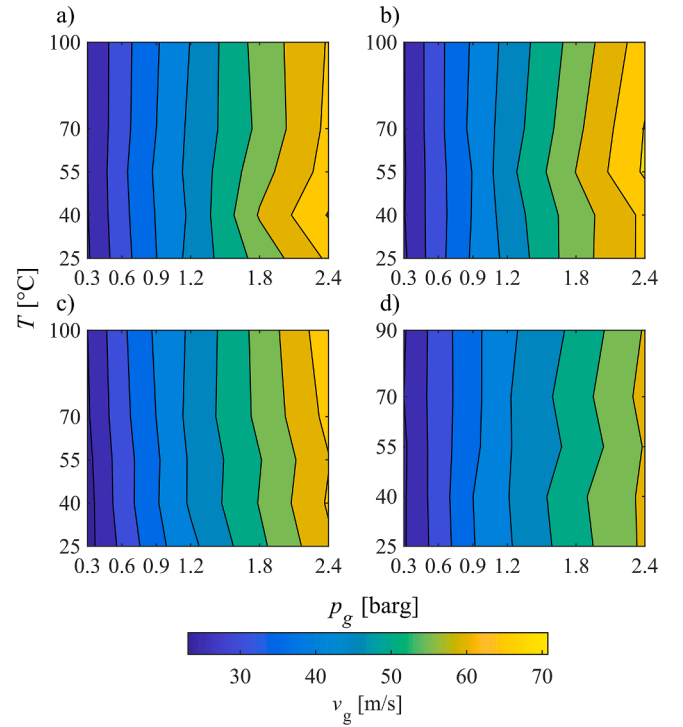


Fig. 10. Effect of liquid temperature and p_g on v_g at $r = 0$ mm and $z = 60$ mm for a) diesel fuel, b) LHO, c) RO, and d) water.

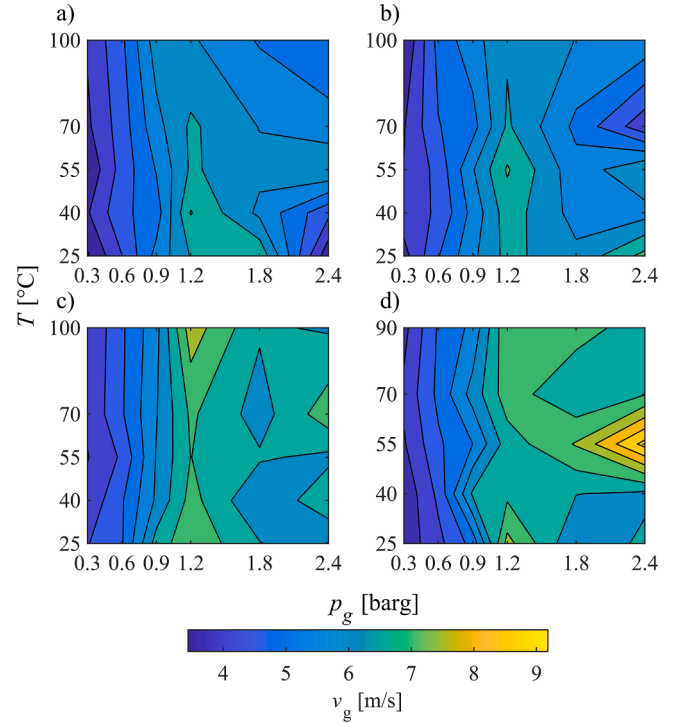


Fig. 11. Effect of liquid temperature and p_g on v_g at $r = 14$ mm and $z = 60$ mm for a) diesel fuel, b) LHO, c) RO, and d) water.

for, e.g., PS and EFF atomizers, where there is no discharging single-phase gas jet. According to (Boersma et al., 1998), $30 \cdot d_h$ is a generally accepted distance in jet flows, beyond which both the mean and the root mean square velocity become self-similar. This is a reasonable relaxation distance in atomization since discharging jets are present in all practical

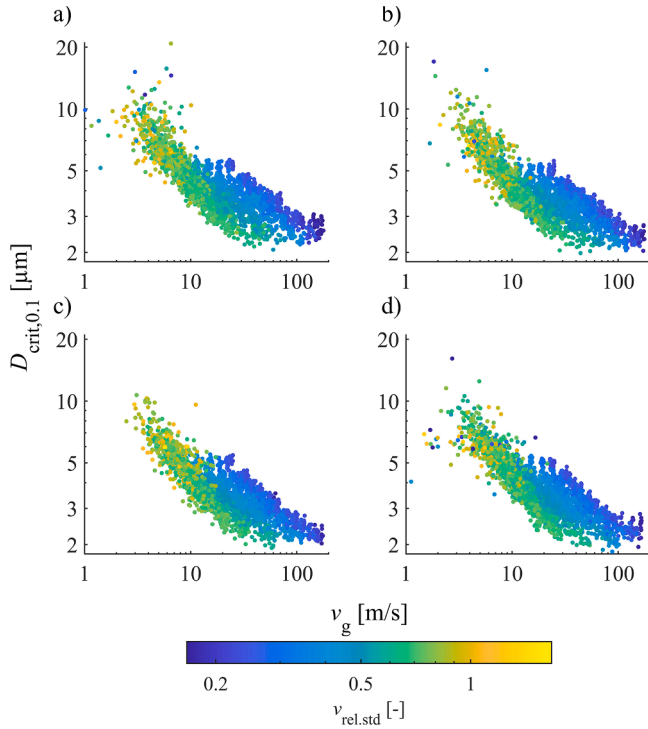


Fig. 12. Critical droplet size-gas velocity distribution for all conditions of AB a) diesel fuel, b) LHO, c) RO, and d) water, colored by $v_{rel,std}$. Note the log scale.

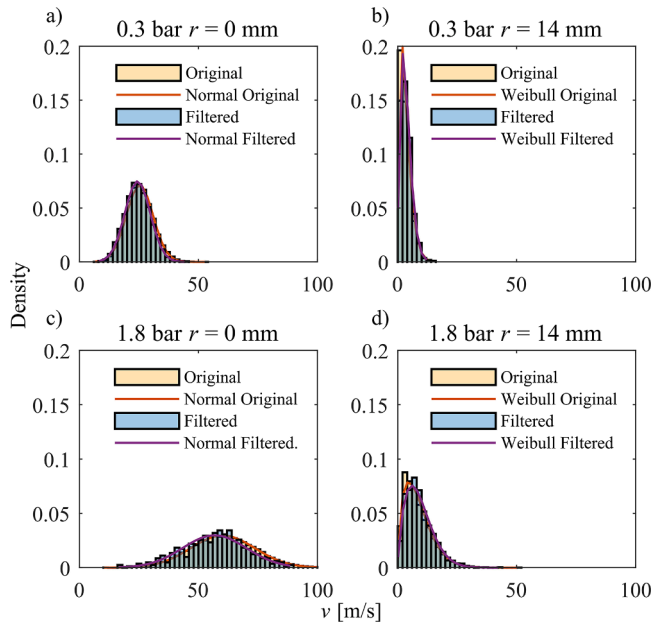


Fig. 13. Original and filtered velocity distributions at a) $p_g = 0.3$ bar, $z = 60$ mm, and $r = 0$ mm, b) $p_g = 0.3$ bar and $r = 14$ mm, c) $p_g = 1.8$ bar and $r = 0$ mm, d) $p_g = 1.8$ bar and $r = 14$ mm.

atomizer types. Therefore, this choice is an ultimate characteristic length scale. In the case of AB, d_h of the annular air jet was considered since the high-velocity air jet governs atomization.

The Stk values of this paper and the work of Lau et al. (Lau and Nathan, 2016) are similar. They considered the diameter of a pipe with two-phase flow discharging as the characteristic dimension, 12.7 mm. It quantitatively matched $30 \cdot d_h$ of our case, which was 12 mm. They

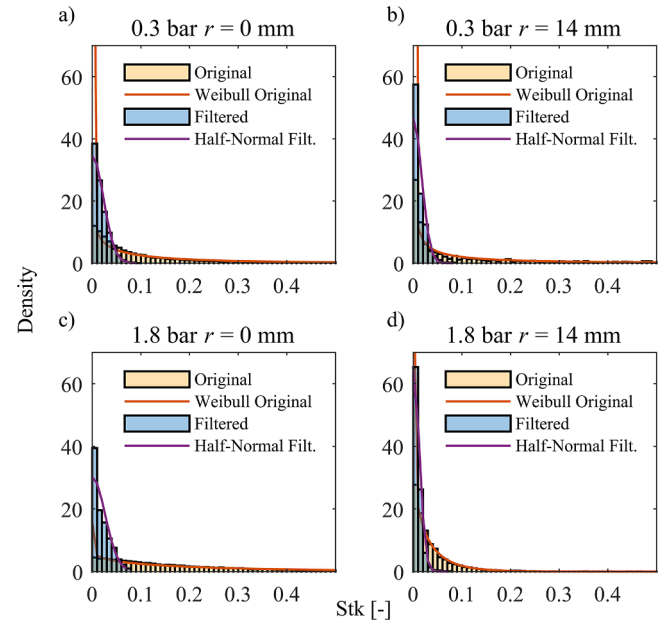


Fig. 14. Original and filtered Stokes number distributions at $z = 60$ mm and a) $p_g = 0.3$ bar and $r = 0$ mm, b) $p_g = 0.3$ bar and $r = 14$ mm, c) $p_g = 1.8$ bar and $r = 0$ mm, d) $p_g = 1.8$ bar and $r = 14$ mm.

assumed that the $10 \mu\text{m}$ droplets are sufficiently small to track the flow at $Stk = 0.3$, while the velocity curves at the lowest Stk did not collapse into one, suggesting that the $Stk < 0.3$ should be investigated. Maintaining these conditions implies that $D < 10 \mu\text{m}$ is necessary; however, smaller particles are becoming increasingly harder to detect by PIV properly (Lau and Nathan, 2016). A further conclusion is that the Stk values decrease by about a magnitude if the characteristic length is the radial width of the jet, where the peak velocity decreases to its half. Therefore, the proper definition of Stk is a critical task, which is frequently overlooked, and the most easy-to-use formula is employed instead to get to the results quickly.

3. Results and discussion

Firstly, the determination of D_{crit} is presented for AB since the corresponding measurements covered the widest range of conditions, and the method was elaborated based on this database. Then the Stokes number criterion is checked based on the experimental data at selected conditions. The $D_{crit,0.1}$ results are presented for all tested liquids and conditions at the center and the periphery. The second subsection shows the effect of filtering for $D_{crit,0.1}$ on the velocity and Stk distributions. Finally, the method is validated on PS and EFF atomizers in OIL and OIG modes in Subsection 3.3.

3.1. Determining the critical droplet diameter

Figure 2 shows a typical droplet size-velocity distribution at the center and the periphery. The droplets are colored by the magnitude of their Stk to visualize the trends better and present the filtering procedure. The droplet velocity distribution is globally symmetrical up to $D = 18 \mu\text{m}$ in Fig. 2a, while the larger droplets have increasingly higher velocities due to overshooting (Gerbino et al., 2021; Wu et al., 2022). It means that large droplets accelerate slowly in the high-velocity gas stream, while their momentum decays slower than that of the gas jet. Therefore, large droplets possess a higher velocity in downstream regions than smaller droplets, which follow the flow better. This is also expressed by the $Stk \ll 1$ criterion, used generally in the literature. The cut at $D = 28 \mu\text{m}$ is the result of outlier filtering. An irregular size-velocity correlation is shown in Fig. 2b at $r = 14$ mm, the furthest

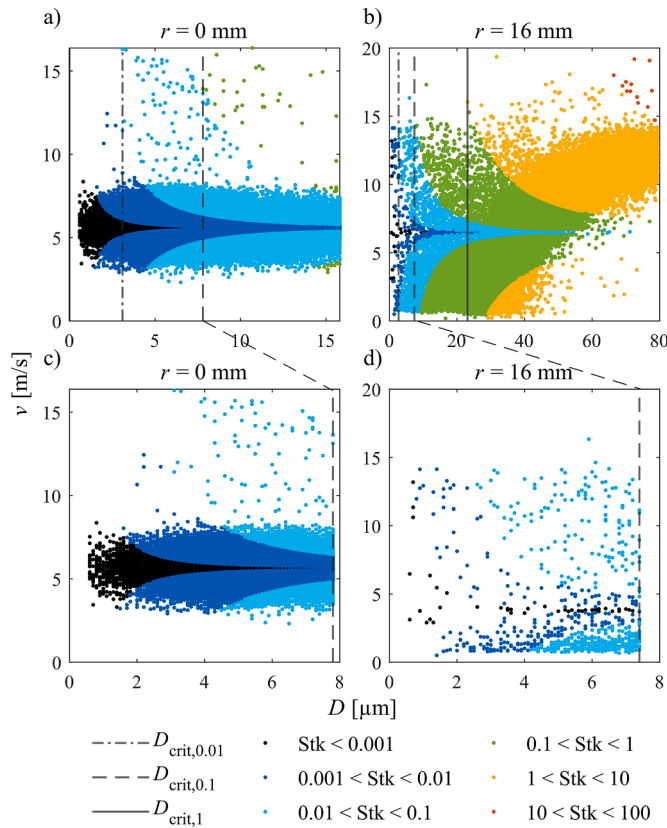


Fig. 15. Droplet size-velocity distribution for pressure swirl atomizer at $p_1 = 5$ bar at $z = 25$ mm. a) $r = 0$ mm, b) $r = 16$ mm, c) $r = 0$ mm filtered by $D_{\text{crit},0.1}$ and d) $r = 16$ mm filtered by $D_{\text{crit},0.1}$.

measured point at $z = 60$ mm for AB. The velocity distribution is asymmetric, even at the smallest droplet sizes. The pre-filtering here rejected the $D > 50 \mu\text{m}$ droplets. Figures 2c and 2d show the cut at $\text{Stk} < 0.1$ enlarged, which was the criterion for filtering for sufficiently small droplets. v_g equals the mean of this residual data set, being a constant value, characterizing a single PDA measurement point. Even the largest droplets might bear $\text{Stk} \sim 0$ if their actual velocity is close to v_g . However, this does not make them follow the flow well. Therefore, the $D_{\text{crit},0.1}$ cuts are performed after sorting the droplets by size, i.e., the diameter of the largest droplet with $\text{Stk} < 0.1$. $D_{\text{crit},0.01}$ and $D_{\text{crit},1}$ are both calculated for reference, shown by vertical lines in Figs. 2a and 2b. The method is the same, but the Stk limit for the filtering was 0.01 and 1, respectively. These critical diameter values appear in later figures to evaluate the appropriateness of the cut with $\text{Stk} < 0.1$.

Estimation of v_g can only be performed on a sufficiently large data set. This is especially critical in the small droplet sizes – in a relative sense – to avoid excessive oscillations and slow and cumbersome data processing, which is present if the data set is read droplet-by-droplet after sorting them in ascending order. For this reason, droplet classes were defined, which contain sufficient data for v_{mean} calculation. This problem is analogous to the creation of histograms. Neither too small nor too large bin size is suitable to visualize the behavior of a random variable. In the current case, the v_{mean} calculation was performed in steps by considering each droplet up to the given size limit. The result is shown in Fig. 3, using various droplet classes, following a Renard series. This approach is commonly used in product family development to cover a wide size range with a sufficiently small number of products, such as standard tube sizes. However, a constant value cannot be used since Fig. 3a contains 38,715 droplets, while Fig. 3b shows 1420 droplets after pre-filtering. After testing several statistical methods for the adaptive determination of bin numbers, the Rice rule was selected, outperforming

the commonly used square root method and Sturges, Doane, Scott, and Freedman-Diaconis formulae. The problem with failed ones was either the number of bins was too high for large data sets (central region) or too low for small data sets (peripheral region). The Rice rule is defined as:

$$b = 2 \cdot n^{1/3}, \quad (4)$$

where n is the number of droplets and b is the number of bins, which was rounded to the nearest integer before use. The result is 67 for Fig. 3a and 22 for Fig. 3b, marked by a thick dashed red line. The difference between the various classes was negligible from $7 \mu\text{m}$ here; hence, the right side of the plot was cut. $D_{\text{crit},0.1}$ is mostly below this value; therefore, this step was critical in the analysis presented further. The droplet velocity distribution can be properly estimated by a two-parameter probability density function, which will be presented in Subsection 3.2. Therefore, v_{std} values are shown for a central and a peripheral region in Fig. 3b and 3d, corresponding to Fig. 3a and 3c. These results also support the choice of the Rice rule since the selected number of bins is sufficient to appropriately follow the global trends and shave the local peaks at both the center and the periphery, which are local outliers and not part of the global trend.

The choice of $D_{\text{crit},0.1}$ is justified in Figs. 4 and 5. Using the Rice rule, they show v_{mean} and v_{std} for various conditions up to a given droplet size class. The result of v_{std} is identical to the root mean square function if that considers the fluctuations around the mean. However, the proper choice of the mean is v_g in multiphase flows, which is to be determined. Therefore, the fluctuating components are presented in this paper only via v_{std} , clearly showing the biased trends if large droplets are also considered. The three markers represent $\text{Stk} = 0.01$ (\diamond), 0.1 (\times), and 1 (\circ). The choice of a very small Stk is not the preferred way to determine D_{crit} since the considered number of droplets could be either insufficient or unrepresentative. Consequently, their velocity may scatter significantly, especially at the periphery. In cases where the circle marker, representing $D_{\text{crit},1}$, is absent, all the droplets possess Stk below 1 due to low velocities in that particular data set. In the spray periphery, the $D_{\text{crit},0.01}$ values are lower than the upper diameter limit of the first droplet class. Consequently, the diamond marker can also be absent from the curves.

The goal is to get an acceptable estimate of an extreme value after the initial transient due to the low number of droplets before overshooting distorts v_{mean} positively or negatively. These effects dominate at higher p_g values, meaning more intense turbulence due to the higher air discharge velocities. The $\text{Stk} = 0.1$ closely hits the point from where v_{mean} and v_{std} feature low variation with increasing droplet size limits at $r = 0$ mm, while this feature was not captured at $r = 14$ mm, which is an irregular data set featuring a high scatter in both velocities and droplet sizes. In the case of v_{std} , shown in Fig. 5., $\text{Stk} = 0.1$ nearly hits the extreme values.

The reason for the superiority of the $\text{Stk} = 0.1$ limits can be concluded by combining Figs. 2, 4, 5, droplet breakup mechanisms (Lefebvre and McDonell, 2017), and turbulence. A problem with filtering for tiny droplets is that they could be satellite droplets of a breakup, meaning a probable clustering with large droplets, biasing v_g estimation (Acharya et al., 2021). In this case, they represent only a fraction of the turbulent fluctuations. This is why the filtering procedure for small droplet sizes could fail in estimating v_g and why the standard deviation is low here. Upon representing the entire turbulent spectrum, v_{std} will peak. However, this criterion alone is insufficient since the peaks at the periphery correspond to extremely high Stk values. The peak is only present because mid-sized droplets could follow the flow better and may possess excessive velocity due to overshooting. Consequently, there is no ultimate tool for a reliable estimation of v_g when the data set is irregular, containing a low number of samples and droplets originating from different breakup processes and different parts of the spray. The decrease then increases of v_{std} and the increase/decrease of v_{mean} , depending on the conditions and spatial location, are clearly

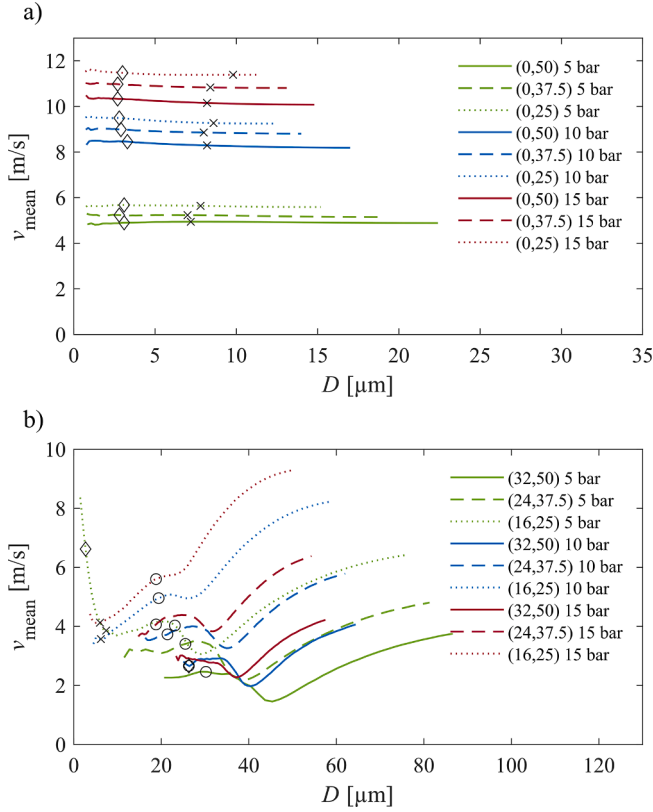


Fig. 16. v_{mean} of droplet classes up to an increasing droplet diameter value. a) $r = 0$ mm and b) various r values to follow the spray cone. Markers: \diamond $D_{\text{crit},0.1}$, \times $D_{\text{crit},0.1}$, and \circ $D_{\text{crit},1}$.

affected by the increasing Stk , meaning that the droplets follow a ballistic path to a growing extent. A further conclusion from the above is that the increase in sample size will not ultimately provide a better estimate of v_g via a reduced sample size since the number of data points will increase, but the size-velocity correlation will be the same, i.e., the information content of the measurement data will not increase further.

The $\text{Stk} = 0.1$ criterion is acceptable based on the above reasoning, and no further adjustment would lead to better results since the minima in Figs. 4a and 4b are slightly underestimated and slightly overestimated in Fig. 4f, and numerous similar examples exist, which are not presented here. Even though it is intuitive, it is essential to perform the PDA measurements symmetrically to avoid velocity bias related to the technique (Lizal et al., 2018).

Critical droplet sizes are shown in Fig. 6 for various Stk values in a spray section in the left column, and the right column contains the resulting v_{mean} values. It was presented above that all droplets fulfilled the $\text{Stk} < 1$ criterion at certain points. Therefore, the \circ markers in Fig. 6a represent the largest droplet size, typical at the spray periphery with low flow velocities. Thus, the trends in Fig. 6a depend mainly on r with a notable increase in $D_{\text{crit},1}$. The central region is flat, and increased p_g leads to higher $D_{\text{crit},1}$ values. As the Stk criterion decreases, D_{crit} becomes flat, as shown in Figs. 6c and 6e, and the effect of p_g also fades, leading to more uniform values. The practical effect of the choice of D_{crit} , and the corresponding Stk limit on v_{mean} is relatively low, as shown in Fig. 6b, d, and f, since the distribution of droplets around v_g was closely uniform up to $\text{Stk} = 1$, shown already in Fig. 2. The crossing trends in Fig. 6f are due to the low number of droplets in the peripheral region, meaning a poor filtering condition.

The relative standard deviation of the velocity, $v_{\text{rel,std}}$, of diesel fuel at $T = 25^\circ\text{C}$ is shown in Fig. 7, which is a similar quantity to turbulent intensity since v_{std} is normalized by v_{mean} . This is a more convenient quantity to express the normalized fluctuations. The first column shows

the unfiltered data, while the second column is the result after filtering using the $D_{\text{crit},0.1}$ criteria, meaning that v_{mean} becomes v_g in the formula of the relative standard deviation in the central region. The results show that even though the fluctuations are the strongest at the center, their relative value increases towards the periphery.

The trends are continuous at $z = 60$ mm, while the peripheral regions deviate from the global trend closer to the nozzle, implying irregularities. The decreasing $v_{\text{rel,std}}$ values with filtering are the direct consequence of removing large droplets, notably affected by overshooting and resulting in more significant overall fluctuations.

Figure 8 shows the effect of two varied parameters, p_g and T , on $D_{\text{crit},0.1}$ for all four investigated liquids of AB at $r = 0$; the results at $r = 14$ mm are shown in Fig. 9. While p_g is dominant, the effect of T and the atomized liquid type is negligible on $D_{\text{crit},0.1}$. Considering that the discharge velocity of the fully expanded jet under adiabatic conditions is 420 m/s at $p_g = 2.4$ bar, the general choice of $D_{\text{crit}} = 3\text{--}5\ \mu\text{m}$ is a working rule of thumb. However, if the number of droplets is low, the result could be notably biased either positively or negatively, depending on the local conditions. Therefore, using identical D_{crit} values for dense and relatively diluted, low-velocity spray regions may lead to biased results.

The corresponding v_g values to Figs. 8 and 9 are shown in Figs. 10 and 11, respectively. The trends match with small deviations from the expected trend of vertical lines at the center, meaning that p_g governs the velocity field. The relatively low values of diesel fuel at the periphery compared to the center is due to this liquid showing the smallest spray cone angle, as discussed in a preceding work (Urbán et al., 2020b). Moreover, the governing effect of p_g is not evident due to the irregular data sets.

Figure 12 shows the ultimate result of the variation of $D_{\text{crit},0.1}$ as a function of v_g , including all measurement points. Based on the definition of Stk , $D_{\text{crit},0.1}$ follows a hyperbole as a function of v_g , which becomes a line with a -45° slope in a log-log plot. The values scatter between 1.8 and 20.8 μm . Considering the data of the developed spray at $z = 60$ mm (Urbán et al., 2019), these boundaries are 2.7 and 10.6 μm . Even though the AB measurement campaign focused on high-velocity atomization, the peripheral regions feature low v_g , which is common in numerous practical atomizers. Therefore, the practical recommendation here is that if v_g is above 10 m/s, $D_{\text{crit},0.1}$ ranges between 2 and 5 μm , which seems a small size range, but a slight bias could be present if a rule of thumb is used instead of calculating $D_{\text{crit},0.1}$. Considering Fig. 7, the large $D_{\text{crit},0.1}$ values corresponds to low v_g . These points represent the periphery with very few exceptions, where the spray is less regular, indicated by high $v_{\text{rel,std}}$ values.

3.2. Velocity and Stokes number distributions

The AB data already contains tiny droplets; therefore, the difference between v_g and v_{mean} is small. This is supported by the normalized histogram, shown in Fig. 13. The original and filtered velocity distributions in the case of two measurement points and two atomizing pressures closely follow each other. The central region, including $r = 0$ mm, shows normal distributions and becoming left-skewed towards the periphery. It is due to the radially asymmetric interaction between the liquid and the gas phases and with the ambient gas. This behavior can be best described by unimodal distributions containing an exponential term. The filtering method does not bias the distributions significantly; therefore, its physical content is intact. This is a critical remark, confirming that the essential details of the turbulent fluctuations were not altered.

Figure 14 shows Stk before and after filtering under the same conditions as Fig. 13. These histograms follow a half-normal distribution after filtering, characterizing simple, natural phenomena. In contrast, the original data is best described by the Weibull (generalized Rosin-Rammler) distribution. Hence, it can be concluded that the filtering method is excellent in confining the relevant flow characteristics and removing the droplets causing irregularities. With increasing p_g , the distribution of the original (pre-filtered) data stretches to higher values

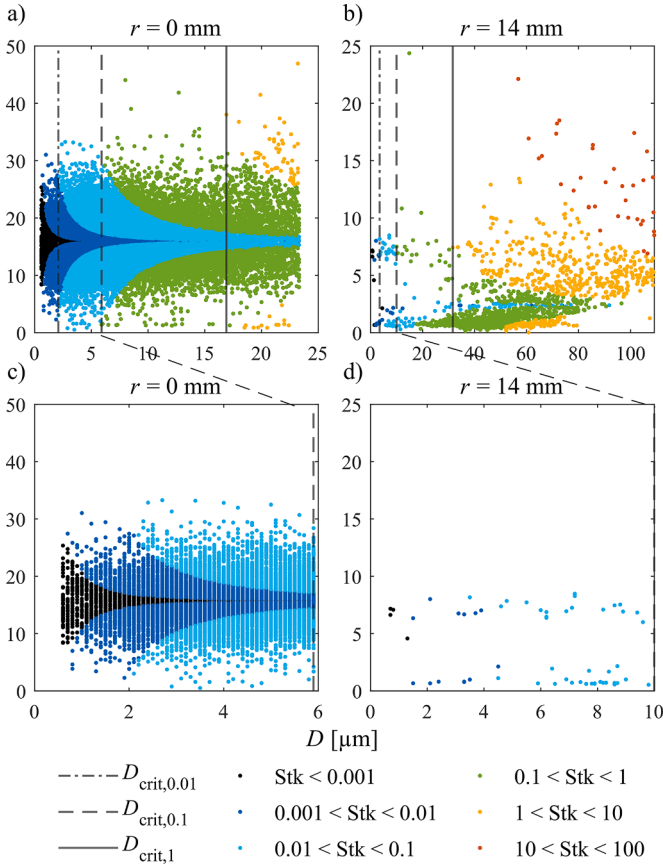


Fig. 17. Droplet size-velocity distribution EFF OIL at $GLR = 0.025$ at $p_g = p_l = 0.7$ bar at $z = 40$ mm. a) $r = 0$ mm, b) $r = 14$ mm, c) $r = 0$ mm filtered by $D_{crit,0.1}$ and d) $r = 16$ mm filtered by $D_{crit,0.1}$.

and becomes flatter since v_g is nearly doubled. At the spray periphery, the distributions are more concentrated around zero as most droplets possess nearly zero velocity magnitude, as shown in Fig. 13. Since numerous larger droplets than $D_{crit,0.1}$ are also rejected, the right tail of the histogram shows a smooth decrease. The left tail remains intact; therefore, the probability of nearly zero Stk values significantly rises, resulting in $P(\text{Stk} < 0.05) > 96\%$ on average for all AB settings.

3.3. Validation: testing the method for other atomizers

The filtering method for v_g was developed for AB; however, due to high velocities, the deviation of v_g from v_{mean} was relatively small in most cases. It was employed unmodified for data sets of other atomizers, which operate notably differently for validation.

3.3.1. Pressure-swirl atomizer

The droplet size-velocity distribution of the PS spray at the center and the periphery is shown in Fig. 15. The central region contains small, slightly slower droplets than the periphery since the discharging liquid from the nozzle follows a hollow-cone shape, and the large droplets follow a ballistic pathway. Apart from several droplets with higher velocity, the inner size-velocity distribution is symmetric around v_g . This is not true for the periphery since the velocity of large droplets uniformly exceed v_g . Even though there is a considerable contrast in droplet sizes, v_g is similar in a cross-section of the spray. This differs from AB data, where v_g dropped from the center towards the periphery.

After filtering by $D_{crit,0.1}$, which value is nearly the same, unlike for AB, the size-velocity distribution remains regular for $r = 0$ mm. However, the distribution is highly asymmetric at $r = 16$ mm. Furthermore, the number of droplets is small here. Due to the high-velocity ballistic

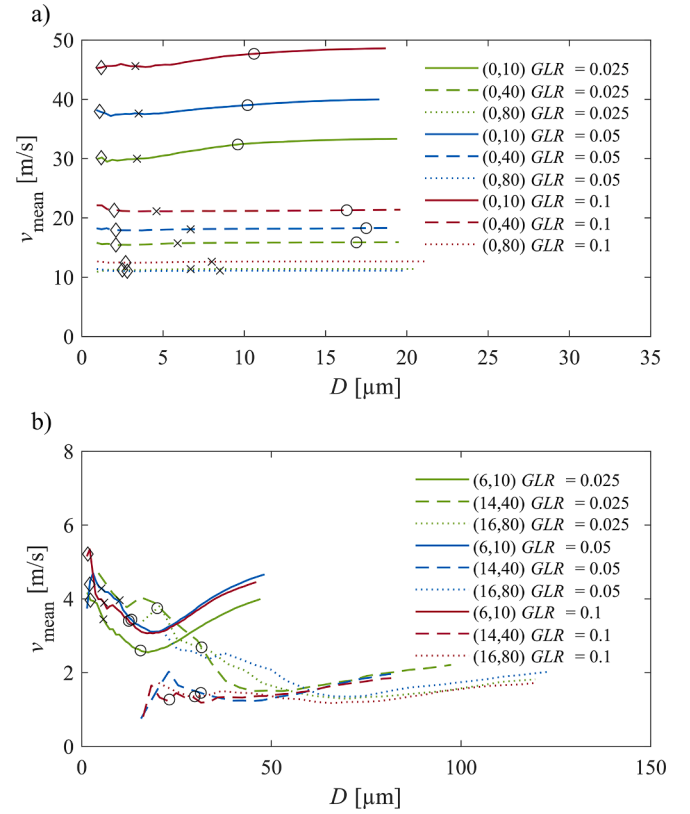


Fig. 18. v_{mean} of droplet classes up to an increasing droplet diameter value of EFF-OIL. a) $r = 0$ mm and b) various r values at the spray periphery. Markers: \diamond $D_{crit,0.01}$, \times $D_{crit,0.1}$, and \circ $D_{crit,1}$.

droplets, $D_{crit,0.1}$ cannot be rationally increased to an alternative value.

v_{mean} as a function of D in Fig. 16a does not vary much since all trends at all $(0, z)$ coordinates are closely flat, unlike in the case of AB. Therefore, v_g can be fairly estimated here even with using all data. The reason is the following. v_g is low, and there are primarily small droplets. Stk of all droplets fall below unity; therefore, the circle marker is not present in any curve in Fig. 16a. $v_{rel, std}$ of PS is identical to AB with the exception that its value drops to almost zero at the outmost measurement points. The corresponding figure is available as supplementary material.

Uneven distribution around v_g (the majority of the droplets are off the axis region) and a low number of samples combined are generally unfortunate for statistical analysis, including the localization of $D_{crit,0.1}$. However, the method works well, as shown in Fig. 16b. Generally, $D_{crit,0.1}$ is between 5 and 10 μm , in line with the frequently used constant values in the literature. However, the denser spray region features a significant variation in v_g at low $D_{crit,0.1}$ values. Therefore, using a rule of thumb threshold might lead to a bias in the range of 100%. $D_{crit,0.1}$ increases with p_l in the center, while this trend is the opposite in the denser spray region. The spray contains no droplet below $\text{Stk} = 0.1$ from $z = 37.5$ mm, meaning that the estimation of v_g is cumbersome in this region; even the smallest droplet class seems to fail following the flow. There can be sufficiently small droplets, but their number is too low. Consequently, an artificial seeding might be necessary for such regimes to estimate v_g correctly.

3.3.2. Effervescent atomizer – out-in-liquid setup

Figure 17 presents the droplet size-velocity distribution of EFF-OIL. The central spray regime shows a relatively high symmetry to v_g and smaller droplet sizes. At the same time, the peripheral region is asymmetric and features large droplets, similar to PS data in Fig. 15. The low number of filtered droplets in the spray periphery implies a possible bias

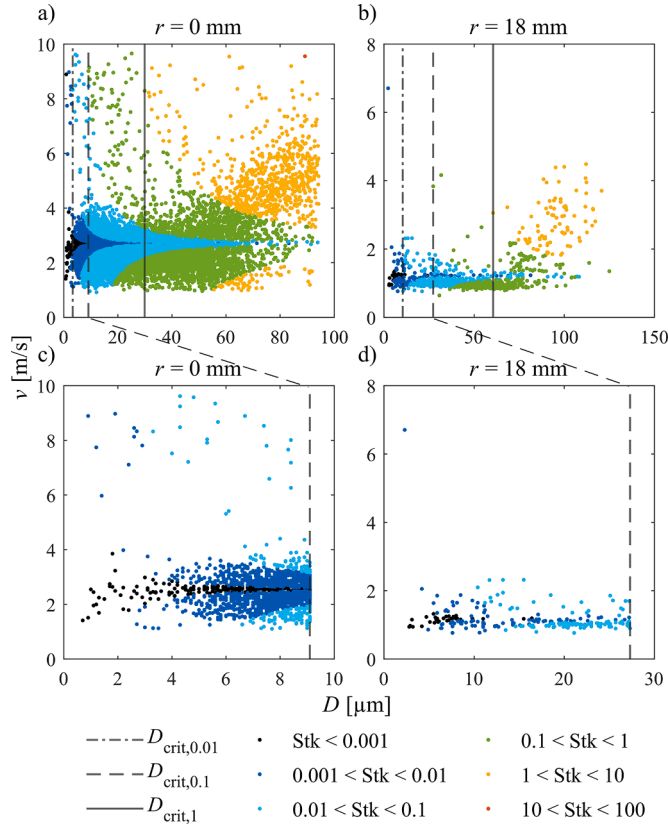


Fig. 19. Droplet size-velocity distribution EFF-OIG at $GLR = 0.05$ at $p_g = p_l = 0.7$ bar at $z = 100$ mm. a) $r = 0$ mm, b) $r = 18$ mm, c) $r = 0$ mm filtered by $D_{crit,0.1}$ and d) $r = 16$ mm filtered by $D_{crit,0.1}$.

in determining v_g . The discrete vertical lines in Fig. 17c are the consequence of the PDA setup, which was focused on a wide droplet size range, while the filtering retains relatively tiny droplets only.

Even at large droplet sizes, the symmetrical size-velocity data at the

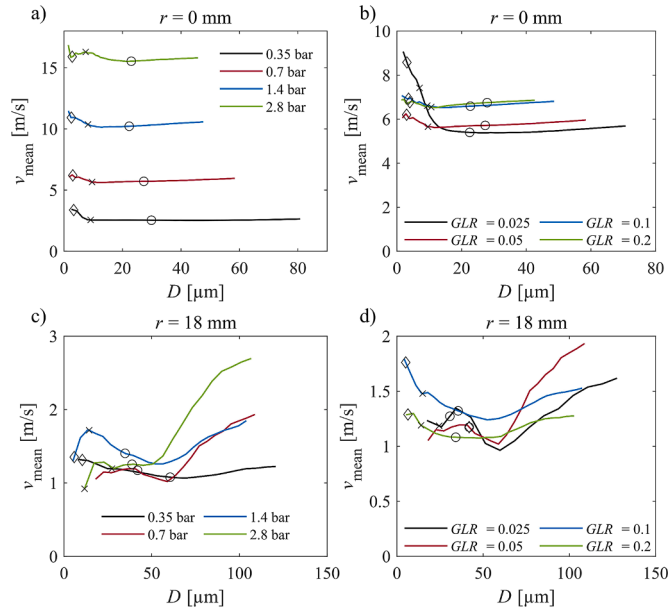


Fig. 20. v_{mean} of droplet classes up to an increasing D value of EFF-OIG at $z = 100$ mm. a) $r = 0$ mm and $GLR = 0.05$, b) $r = 0$ mm and $p_g = p_l = 0.7$ bar c) $r = 18$ mm and $GLR = 0.05$, and d) $r = 18$ mm and $p_g = p_l = 0.35$ bar. \diamond $Stk = 0.01$, \times $Stk = 0.1$, and \circ $Stk = 1$.

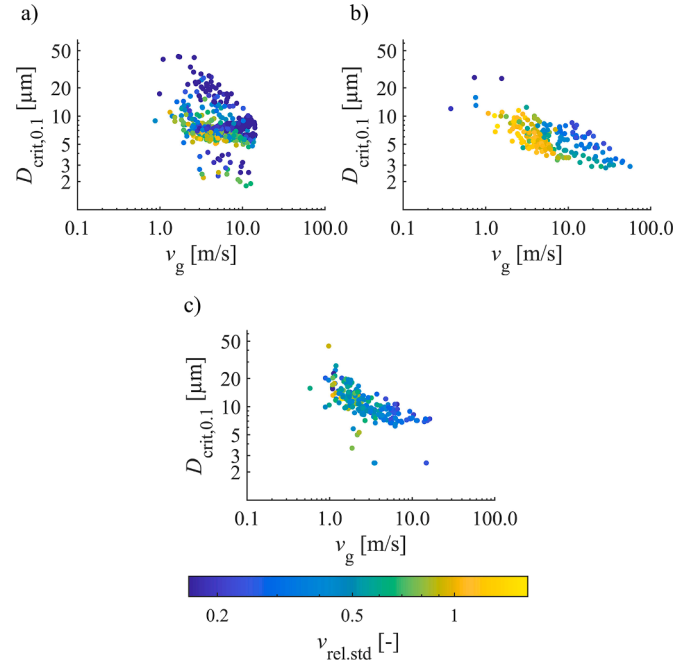


Fig. 21. Critical droplet size-gas velocity distribution for all conditions of a) PS, b) EFF-OIL, and c) EFF-OIG atomizers, colored by $v_{rel,std}$. Note the log-log scale.

spray center suggest that v_{mean} varies only slightly with the threshold. Therefore, the probability of high bias due to improper $D_{crit,0.1}$ estimation is low, as shown in Fig. 18a. The trends follow the general behavior of a discharging circular jet: the velocities are notably higher at $r = 0$ mm close to the nozzle. The resulting $D_{crit,0.1}$ values range from 3 to 7.5 μ m. The $Stk = 0.1$ works here well for determining D_{crit} . However, this is not true at the periphery due to the low number of droplets, as shown in Fig. 18b.

The $Stk = 1$ seems a better choice here to capture the minima of v_{mean} , partially due to the larger number of considered droplets, which is supported by the v_{std} data included in the supplementary material. Nevertheless, this choice does not work uniformly well. Interestingly, even the smallest droplet class here exceeds $Stk = 0.1$, similar to PS data in Fig. 16. It means that there is an insufficient number of small droplets that fulfill the $Stk < 0.1$ criteria. Higher GLR values lead to higher v_{mean} values at $r = 0$ mm, up to $z = 40$ mm, and this trend flips at $z = 80$ mm for $GLR = 0.025$ and 0.05 . Due to the low velocities and the overshooting of large droplets at the periphery, the mixed trends do not allow to make general conclusions, similar to AB and PS atomizers.

3.3.3. Effervescent atomizer – out-in-gas setup

The droplet size-velocity distribution of EFF-OIG is shown in Fig. 19. In this case, the droplets are large at both the center and the periphery; furthermore, the distributions are asymmetric. Overshooting is clearly present since the large droplets follow a ballistic pathway. In this atomizer, the scatter of the droplet velocity is lower at the periphery, while several small droplets possess a higher velocity at the center. Nevertheless, the number of droplets is also larger here. Due to the low velocities, $D_{crit,0.1}$ is sufficiently large, especially at the periphery, almost reaching 30 μ m.

The proposed estimation method of $D_{crit,0.1}$ works well at $r = 0$ mm, as shown in Fig. 20a and 16b. These v_{mean} trends are qualitatively similar to AB, as shown in Fig. 4a. $D_{crit,0.1}$ is around 10 μ m at $r = 0$ mm, and lower values may contain notable bias. The $Stk = 1$ criterion at the periphery provides a better estimation for v_g , similar to the EFF-OIL atomizer. However, the minima of the N-shaped trends vary. The corresponding $D_{crit,0.1}$ is not presented at $GLR = 0.05$, $r = 18$ mm, and $p_g = p_l = 0.7$ bar since the number of droplets is too low below $Stk = 1$, which

was also noticeable in Fig. 19d. $D_{\text{crit},0.1}$ otherwise falls between 10 and 30 μm at $r = 18$ mm. The $v_{\text{rel},\text{std}}$ trends of both EFF-OIG and OIL setups are identical to that of AB, i.e., the central region is characterized by low $v_{\text{rel},\text{std}}$, while its value increases towards the periphery. The corresponding figures are available in the supplementary material.

$D_{\text{crit},0.1}$ for all evaluated conditions of the three atomizer configurations are shown in Fig. 21. The lowest ultimate boundary of $D_{\text{crit},0.1}$ is similar to that of Fig. 12; However, the spread is significantly larger. It ranges from 1.8 to 43.3 μm for PS, 2.8–25.8 μm for EFF-OIL, and 2.5–44.4 μm for EFF-OIG. Values above 10 μm are confined to $v_g < 10$ m/s, which agrees with the results plotted in Fig. 12; only the $D_{\text{crit},0.1}$ was doubled. Since low values are present even at the lowest velocities, no hyperbole or another curve can be fitted to provide an approximation for a specific atomizer type, which would look like a line with a -45° slope in the log-log plot. It can be concluded that at low velocities, significantly larger droplets, i.e., above 10 μm , can also be used for v_g estimation after careful checking of the D – v_g trends. The behavior of EFF is similar to AB in the sense that the peripheral regions feature the highest $v_{\text{rel},\text{std}}$, while no such correlation is present in the case of PS due to the different spray structures. The only correlation in Fig. 21a is that positions, where $D_{\text{crit},0.1}$ was around 5 μm , $v_{\text{rel},\text{std}}$ is high, meaning intense turbulence.

4. Conclusions

Determination of v_g from PDA data is often performed using a low-pass filter by droplet size, following a rule of thumb, i.e., below 0.9–30 μm , depending on the author. Another generally accepted method for estimating v_g is filtering for $\text{Stk} \ll 1$; however, the definitions for the length scale notably vary in the literature, leading to differences in the range of magnitudes. After revising an extensive PDA database of four practical atomizers, the following conclusions were derived.

- 1 Using a rule of thumb for low-pass filtering might lead to highly biased results for v_g , proven by data from all four investigated atomizers, covering a wide range of setups.
- 2 The length scale was proposed as $30 \cdot d_h$ for Stk calculation, allowing its unbiased determination for, e.g., PS atomizers. Using this definition, the $\text{Stk} = 0.1$ condition for estimating D_{crit} is generally usable for v_g estimation.
- 3 Filtering for too small droplets may lead to biased data for estimating the turbulent characteristics, presented through the variation of v_{std} as a function of droplet sizes. Small droplets may be affected by clustering, and large droplets have considerable inertia and follow a ballistic path. Therefore, neither underestimation nor overestimation of D_{crit} is a safe choice in general.
- 4 At $v_g < 10$ m/s, the $\text{Stk} = 0.1$ threshold results in highly scattered D_{crit} values, ranging from 1.8 μm to 44.4 μm , typical in peripheral regions. Also, the size-velocity distribution is asymmetric here. Therefore, it is advised to determine v_g based on a local extreme value, supported by checking size-velocity correlation maps and v_{std} trends. No generally applicable procedure was found; outliers may behave differently for various atomizers, requiring manual post-processing in irregular spray data sets. In the dense spray region of PS and peripheral regions of EFF, $\text{Stk} = 1$ seemed to be a better estimate for D_{crit} , where the $v_g < 10$ m/s condition is fulfilled.
- 5 The droplets of AB were already small. Hence, filtering affects the velocity histogram marginally. However, filtering for $D_{\text{crit},0.1}$ notably affects the Stk distribution, after which $P(\text{Stk} < 0.05) > 96\%$. Moreover, the turbulent characteristics are better captured, indicated by the half-normal distribution, forming from Weibull after filtering for $D_{\text{crit},0.1}$.
- 6 The database of AB covered a wide range of conditions, including more than two magnitudes spread in liquid viscosity. The liquid type and the preheating temperature have a negligible effect on $D_{\text{crit},0.1}$; it

was ultimately governed by p_g . This is because the atomizing air flow governs the flow field.

The reader can find the used Matlab codes at (Rácz and Józsa, 2022), and the algorithm steps are detailed in Appendix A.

Funding

The research reported in this paper was supported by the Prime Ministry of Hungary via the Human Resource Support Management, grant N^o. NTP-NFTÖ-21-B-0084, János Bolyai Research Scholarship of the Hungarian Academy of Sciences, National Research, Development and Innovation Fund of Hungary, project N^os OTKA-FK 137758, and TKP2020 NC, Grant No. BME-NVA-02 based on the charter of bolster issued by the NRDI Office under the auspices of the Ministry for Innovation and Technology, financed under the TKP2021 funding scheme. The authors acknowledge the financial support from project no. LTAIN19044 funded from the program INTER EXCELLENCE (INTER–ACTION) by the Ministry of Education, Youth and Sports of the Czech Republic.

CRediT authorship contribution statement

Erika Rácz: Conceptualization, Methodology, Software, Validation, Formal analysis, Data curation, Writing – original draft, Writing – review & editing, Visualization. **Milan Malý:** Validation, Investigation, Resources, Data curation, Supervision. **Jan Jedelský:** Resources, Supervision, Project administration, Funding acquisition. **Viktor Józsa:** Conceptualization, Validation, Writing – original draft, Writing – review & editing, Supervision, Project administration, Funding acquisition.

Declaration of Competing Interest

The authors declare that they have no known competing financial interests or personal relationships that could have appeared to influence the work reported in this paper.

Data Availability

Data will be made available on request.

Supplementary materials

Supplementary material associated with this article can be found, in the online version, at doi:10.1016/j.ijmultiphaseflow.2022.104260.

Appendix A

The following algorithm details the procedure of determining v_g , based on the software code available on the homepage of our research group (Rácz and Józsa, 2022). See Fig. A.1 for the flow chart.

- 1 Read the data file(s) to be processed. It should contain at least several thousand droplet size and velocity data pairs. If there are multiple velocity components, calculate the velocity magnitude.
- 2 Filter the data for unreal droplets, i.e., smaller ones than the laser wavelength. Filter the outlier droplets by, e.g., using three times the mean absolute deviation. These are extremely large ones and are statistically not representative. They are the results of physical processes with low likelihood, while they could significantly bias the statistical modeling.
- 3 Select the desired Stk value; 0.1 is recommended. As an initial step, use the entire spray and estimate v_g as v_{mean} .
 - a Calculate the Stk values.

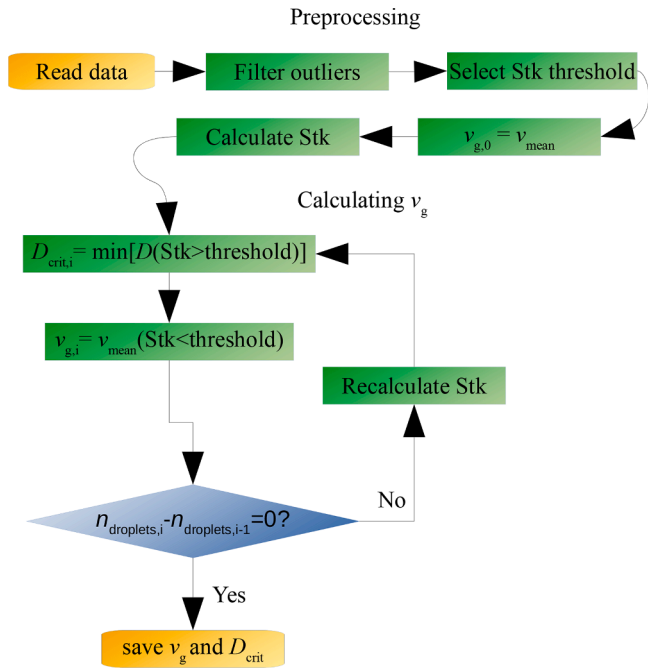


Fig. A.1. Flow chart of the algorithm.

- b Find the smallest droplet with a higher Stk value than the threshold. This is D_{crit} .
 - c Recalculate v_g from the velocity data from the smaller droplets. Recalculate Stk with the new v_g value and find the smallest droplet with a higher Stk value than the threshold again.
 - d Repeat 3.c until convergence. The criterion here is the number of droplets with a lower Stk value than the threshold. This procedure usually takes only a few iterations.
 - e Export the data meeting the $Stk < threshold$ criterion.
- 4 Check if the D_{crit} value is close to the maximum of the standard deviation by cumulatively considering droplet classes, determined by an adaptive function for calculating the number of bins. For instance, use the Rice rule. Create a droplet size-velocity correlation plot and check if the droplets below D_{crit} follow a regular distribution.

This algorithm was tested for a few different atomizers operating by velocity difference for creating the spray. Please, stress this algorithm for your atomizer.

References

- Acharya, A.S., Deevi, S., Dhivayaraja, K., Tangirala, A.K., Panchagnula, M.V., 2021. Spatio-temporal microstructure of sprays: Data science-based analysis and modelling. *J. Fluid Mech.* 912, 1–27. <https://doi.org/10.1017/jfm.2020.1116>.
- Albrecht, H.-E., Borys, M., Damaschke, N., Tropea, C., 2003. *Laser Doppler and Phase Doppler Measurement Techniques*, Laser Doppler and Phase Doppler Measurement Techniques. Springer Berlin Heidelberg, Berlin, Heidelberg. <https://doi.org/10.1007/978-3-662-05165-8>.
- Babinsky, E., Sojka, P.E., 2002. Modeling drop size distributions. *Prog. Energy Combust. Sci.* 28, 303–329. [https://doi.org/10.1016/S0360-1285\(02\)00004-7](https://doi.org/10.1016/S0360-1285(02)00004-7).
- Berni, F., Sparacino, S., Riccardi, M., Cavicchi, A., Postrioti, L., Borghi, M., Fontanesi, S., 2022. A zonal secondary break-up model for 3D-CFD simulations of GDI sprays. *Fuel* 309, 122064. <https://doi.org/10.1016/j.fuel.2021.122064>.
- Boersma, B.J., Brethouwer, G., Nieuwstadt, F.T.M., 1998. A numerical investigation on the effect of the inflow conditions on the self-similar region of a round jet. *Phys. Fluids* 10, 899–909. <https://doi.org/10.1063/1.869626>.
- Broumand, M., Albert-Green, S., Yun, S., Hong, Z., Thomson, M.J., 2020. Spray combustion of fast pyrolysis bio-oils: Applications, challenges, and potential solutions. *Prog. Energy Combust. Sci.* 79, 100834. <https://doi.org/10.1016/j.pecs.2020.100834>.
- Chiong, M.C., Chong, C.T., Ng, J.H., Lam, S.S., Tran, M.V., Chong, W.W.F., Mohd Jaafar, M.N., Valera-Medina, A., 2018. Liquid biofuels production and emissions performance in gas turbines: A review. *Energy Convers. Manag.* <https://doi.org/10.1016/j.enconman.2018.07.082>.

- Chong, C.T., Hochgreb, S., 2015. Effect of Atomizing Air Flow on Spray Atomization of an Internal-Mix Twin-Fluid Atomizer. *At. Sprays* 25, 657–673. <https://doi.org/10.1015/AtomizSpr.2015011361>.
- Collin-Bastiani, F., Riber, E., Cuenot, B., 2021. Study of inter-sector spray flame propagation in a linear arrangement of swirled burners. *Proc. Combust. Inst.* 38, 6299–6308. <https://doi.org/10.1016/j.proci.2020.05.050>.
- de Blas, I., Mediavilla, M., Capellán-Pérez, I., Duce, C., 2020. The limits of transport decarbonization under the current growth paradigm. *Energy Strateg. Rev.* 32. <https://doi.org/10.1016/j.esr.2020.100543>.
- Elghobashi, S., 1994. On predicting particle-laden turbulent flows. *Appl. Sci. Res.* 52, 309–329. <https://doi.org/10.1007/BF00936835>.
- Feng, Z., Tang, C., Yin, Y., Zhang, P., Huang, Z., 2019. Time-resolved droplet size and velocity distributions in a dilute region of a high-pressure pulsed diesel spray. *Int. J. Heat Mass Transf.* 133, 745–755. <https://doi.org/10.1016/j.ijheatmasstransfer.2018.12.147>.
- Ferrand, V., Bazile, R., Borée, J., Charnay, G., 2003. Gas-droplet turbulent velocity correlations and two-phase interaction in an axisymmetric jet laden with partly responsive droplets. *Int. J. Multiph. Flow* 29, 195–217. [https://doi.org/10.1016/S0301-9322\(02\)00151-9](https://doi.org/10.1016/S0301-9322(02)00151-9).
- Gerbino, F., Tretola, G., Morgan, R., Atkins, P., Vogiatzaki, K., 2021. Influence of the initial droplet distribution on the prediction of spray dynamics in Eulerian-Lagrangian simulations. *Int. J. Multiph. Flow* 141, 103642. <https://doi.org/10.1016/j.ijmultiphaseflow.2021.103642>.
- Hannula, I., Reiner, D.M., 2019. Near-Term Potential of Biofuels, Electrofuels, and Battery Electric Vehicles in Decarbonizing Road Transport. *Joule* 3, 2390–2402. <https://doi.org/10.1016/j.joule.2019.08.013>.
- Jedelsky, J., Jicha, M., 2014. Droplet dynamics in internally mixed twin-fluid spray. *WIT Trans. Eng. Sci.* 82, 227–238. <https://doi.org/10.2495/AFM140201>.
- Jedelsky, J., Maly, M., Pinto del Corral, N., Wigley, G., Janackova, L., Jicha, M., 2018. Air-liquid interactions in a pressure-swirl spray. *Int. J. Heat Mass Transf.* 121, 788–804. <https://doi.org/10.1016/j.ijheatmasstransfer.2018.01.003>.
- Kourmatzis, A., Pham, P.X., Masri, A.R., 2013. Air assisted atomization and spray density characterization of ethanol and a range of biodiesels. *Fuel* 108, 758–770. <https://doi.org/10.1016/j.fuel.2013.01.069>.
- Lau, T.C.W., Nathan, G.J., 2016. The effect of Stokes number on particle velocity and concentration distributions in a well-characterised, turbulent, co-flowing two-phase jet. *J. Fluid Mech.* 809, 72–110. <https://doi.org/10.1017/jfm.2016.666>.
- Lefebvre, A.H., McDonnell, V.G., 2017. *Atomization and Sprays*, Second. CRC Press, Boca Raton, FL.
- Li, Q., Peng, Z., Liu, L., Chen, S., Liu, J., Wang, L.P., Liu, T., Wang, G., 2021. A comparison of different methods for estimating turbulent dissipation rate in under-resolved flow fields from synthetic PIV images. *Chem. Eng. Res. Des.* 175, 161–170. <https://doi.org/10.1016/j.cherd.2021.09.004>.
- Lizal, F., Jedelsky, J., Morgan, K., Bauer, K., Llop, J., Cossio, U., Kassinos, S., Verbanck, S., Ruiz-Cabello, J., Santos, A., Koch, E., Schnabel, C., 2018. Experimental methods for flow and aerosol measurements in human airways and their replicas. *Eur. J. Pharm. Sci.* 113, 95–131. <https://doi.org/10.1016/j.ejps.2017.08.021>.
- MathWorks, 2020. MATLAB, Release 2020b.
- Menon, S., Gurunadham, M., 2022. Droplet behavior in overexpanded supersonic two-phase jets. *Int. J. Multiph. Flow* 152, 104076. <https://doi.org/10.1016/j.ijmultiphaseflow.2022.104076>.
- Nasr, G.G., Yule, A.J., Bendig, L., 2002. *Industrial Sprays and Atomization*, 2nd ed. Springer-Verlag London Ltd., London. <https://doi.org/10.1007/978-1-4471-3816-7>.
- Pakhomov, M.A., Terekhov, V.I., 2020a. Numerical analysis of swirling turbulent droplet-laden flow and heat transfer in a sudden pipe expansion. *Int. J. Heat Fluid Flow* 85, 108681. <https://doi.org/10.1016/j.ijheatfluidflow.2020.108681>.
- Pakhomov, M.A., Terekhov, V.I., 2020b. Numerical analysis of swirling turbulent droplet-laden flow and heat transfer in a sudden pipe expansion. *Int. J. Heat Fluid Flow* 85, 108681. <https://doi.org/10.1016/j.ijheatfluidflow.2020.108681>.
- Panão, M., 2020. Post-processing large PDI data application to sprays. 8th International Advanced Course on Liquid Interfaces, Drops and Sprays - LIDESP. <https://doi.org/10.13140/RG.2.2.18081.02402>. Online.
- Rácz, E., Józsa, V., 2022. Software codes by the BME combustion Research Group [WWW Document]. URL <https://crg.energia.bme.hu/software/> (accessed 4.27.22).
- Sepúlveda, N.A., Jenkins, J.D., de Sisternes, F.J., Lester, R.K., 2018. The Role of Firm Low-Carbon Electricity Resources in Deep Decarbonization of Power Generation. *Joule* 2, 2403–2420. <https://doi.org/10.1016/j.joule.2018.08.006>.
- Sommerfeld, M., Kussin, J., 2003. Analysis of collision effects for turbulent gas-particle flow in a horizontal channel. Part II. Integral properties and validation. *Int. J. Multiph. Flow* 29, 701–718. [https://doi.org/10.1016/S0301-9322\(03\)00033-8](https://doi.org/10.1016/S0301-9322(03)00033-8).
- Temme, J.E., Allison, P.M., Driscoll, J.F., 2014. Combustion instability of a lean premixed prevaporized gas turbine combustor studied using phase-averaged PIV. *Combust. Flame* 161, 958–970. <https://doi.org/10.1016/j.combustflame.2013.09.021>.
- Urbán, A., Groniewsky, A., Malý, M., Józsa, V., Jedelský, J., 2020a. Application of big data analysis technique on high-velocity airblast atomization: Searching for optimum probability density function. *Fuel* 273, 117792. <https://doi.org/10.1016/j.fuel.2020.117792>.
- Urbán, A., Katona, B., Malý, M., Jedelský, J., Józsa, V., 2020b. Empirical correlation for spray half cone angle in plain-jet airblast atomizers. *Fuel* 277, 118197. <https://doi.org/10.1016/j.fuel.2020.118197>.
- Urbán, A., Malý, M., Józsa, V., Jedelský, J., 2019. Effect of liquid preheating on high-velocity airblast atomization: From water to crude rapeseed oil. *Exp. Therm. Fluid Sci.* 102, 137–151. <https://doi.org/10.1016/j.expthermflusci.2018.11.006>.

- Wu, H., Zhang, F., Zhang, Z., Hou, L., 2022. Atomization and droplet dynamics of a gas-liquid two-phase jet under different mass loading ratios. *Int. J. Multiph. Flow* 151, 104043. <https://doi.org/10.1016/j.ijmultiphaseflow.2022.104043>.
- Xiao, G., Zhou, T., Ni, M., Chen, C., Luo, Z., Cen, K., 2014. Study on oscillating flow of moderate kinetic Reynolds numbers using complex velocity model and phase Doppler anemometer. *Appl. Energy* 130, 830–837. <https://doi.org/10.1016/j.apenergy.2014.02.005>.
- Xu, D., Chen, J., 2013. Accurate estimate of turbulent dissipation rate using PIV data. *Exp. Therm. Fluid Sci.* 44, 662–672. <https://doi.org/10.1016/j.expthermflusci.2012.09.006>.
- Zaremba, M., Kozák, J., Malý, M., Weiß, L., Rudolf, P., Jedelský, J., Jícha, M., 2018. An experimental analysis of the spraying processes in improved design of effervescent atomizer. *Int. J. Multiph. Flow* 103, 1–15. <https://doi.org/10.1016/j.ijmultiphaseflow.2018.01.012>.
- Zaremba, M., Weiß, L., Malý, M., Wensing, M., Jedelský, J., Jícha, M., 2017. Low-pressure twin-fluid atomization: Effect of mixing process on spray formation. *Int. J. Multiph. Flow* 89, 277–289. <https://doi.org/10.1016/j.ijmultiphaseflow.2016.10.015>.